
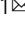




Flipping the helicity of X-rays from an undulator at unprecedented speed

Karsten Holldack¹  , Christian Schüssler-Langeheine¹, Paul Goslawski¹, Niko Pontius¹, Torsten Kachel¹, Felix Armbrorst¹ , Markus Ries¹, Andreas Schällicke¹, Michael Scheer¹, Winfried Frentrup¹ & Johannes Bahrtd¹ 

X-ray circular dichroism (XMCD), one of the main tools to study magnetism, benefits enormously from the capability of a fast alterable helicity of circularly polarized X-ray photons. Here we present a method for boosting the alternating frequency between right- and left-handed photons to the MHz regime, more than three orders of magnitude faster than state-of-the-art technologies. The method is based on a twin elliptical undulator installed in an electron storage ring being operated in a novel mode where the electron optics is tuned close to a resonance with electrons captured in transverse resonance island buckets. Propagating through the twin undulator, electrons from different islands emit photons of the same wavelength but of opposite helicity. These two helicity components can be alternated as fast as 2 ns. In a proof-of-principle experiment at BESSY II, we demonstrate XMCD at the $L_{2,3}$ absorption edges of Ni with an 800 ns helicity flip.

¹ Helmholtz-Zentrum Berlin für Materialien und Energie, Albert-Einstein-Strasse 15, D-12489 Berlin, Germany. email: karsten.holldack@helmholtz-berlin.de, johannes.bahrtd@helmholtz-berlin.de

Over the past decades, X-ray circular dichroism (XMCD)^{1–3}, the difference in absorption of the left and right circularly polarized X-rays in magnetic material, has become an indispensable tool to study element-selective static and dynamic magnetism on magnetic recording materials^{4,5}, quantum materials^{6,7}, clusters⁸, as well as molecular materials relevant for spintronics and catalysis⁹. To measure XMCD, absorption spectra across atomic resonances are recorded with different relative orientation of X-ray helicity and sample magnetization. Sum rules relate integrals over the XMCD spectrum, i.e., the difference between these spectra, to the ordered spin and orbital magnetic moment¹⁰. At synchrotron light sources, insertion devices producing circularly polarized X-rays¹¹ have been successfully employed, combined with proper tools at the experiment to manipulate the magnetization of the sample. In most XMCD experiments, the time needed to change the X-ray helicity or the magnetization is longer than the time needed to change the photon energy and to acquire the absorption signal at a certain energy/polarization setting. As the slow processes determine the time needed for the experiment, typically two energy-dependent spectra are recorded subsequently with a helicity or magnetization change in between. Although this scheme is acceptable when sample and all other experimental parameters are stable over the whole time of the experiment, studies from dynamical processes and experiments addressing small effects such as in molecular spin systems on surfaces, spatially resolved magnetic domains, and quasi-particles in solids¹² significantly benefit from a scheme where very fast helicity alternation in the MHz regime allows for a quasi-simultaneous acquisition of both X-ray helicities such that the XMCD spectrum can be recorded in a single energy sweep. This experimental scheme does not only reduce the total acquisition time per spectrum (allowing, e.g., to study dynamical processes) but also improves the signal-to-noise ratio considerably, because the X-ray pointing stability in modern light sources improves by four to five orders of magnitude¹³ between 0.1 Hz and MHz acquisition frequency, which promises that previously inaccessible effects in magnetism become measurable.

Although practically all XMCD experiments are carried out in the soft X-ray range, where excitations into the $3d$ states of transition metals and $4f$ states of lanthanides occur, a helicity alternation at a rate of 2 kHz has so far only been demonstrated in the hard X-ray regime¹⁴. A diamond crystal-based quarter wave plate behind a planar undulator has been oscillated around the Bragg angle utilizing a galvanometer scanner. Efficient phase retarders are not available for soft X-rays and are also difficult to operate during energy scans. In this energy range, the polarization must be flipped within the undulator.

Today, all accelerator-based light sources with variable polarization are realized either as permanent magnet undulators (PMUs) or as room temperature electromagnetic undulators (EMUs), or as a combination of both technologies¹⁵. Only recently, a superconducting undulator prototype with variable polarization, SCAPE (Superconducting Arbitrarily Polarizing Emitters), was built at the Advanced Photon Source (APS)¹⁶. The alternation frequency of PMUs is limited to a few Hz¹⁷, because magnet arrays must be accelerated in the presence of strong magnetic forces. EMUs are limited in frequency by the coil self-inductance and the eddy currents induced into the vacuum chamber, where the eddy currents can be compensated with dedicated coils¹⁸. The helicity alternation rate of a SCAPE is restricted by the quench behavior of the wire. Double undulator systems that generate both helicities simultaneously can further enhance the alternation frequency. The photon beams of the two undulators can be separated statically, and the selection of the specific helicity is accomplished with a chopper in the beamline close to the focal point. A static separation can be realized as an

angle orbit bump^{19,20} or as an orbit displacement²¹. Alternatively, a dynamic local electron orbit bump in combination with an aperture in the front end chooses the light from one or the other undulator, where both beams are on-axis. A dynamic orbit displacement has been realized with a five kicker bump^{22,23}. In other concepts, the two undulator beams of opposite helicity are alternatively modified to be blocked efficiently with the monochromator bandwidth. This can be accomplished with two methods: (i) phase shifters in one or the other module split the spectrum with zero intensity on resonance via the introduction of phase jumps of π ²⁴; (ii) additional coils on top of the poles detune the undulator harmonic slightly. The latter design is part of the APS upgrade project utilizing two SCAPE undulators (Y. Ivanushenkov, personal communication, 2019). For further details on various undulator technologies, we refer to ref. ²⁰. All coil-based designs are limited to a few 10 Hz and existing chopper systems limit the alternation frequency to about 100 Hz. Recently, MHz choppers²⁵ have been used in soft X-ray beamlines to extract single camshaft bunches from the fill pattern. However, they need a small intermediate focus (not standard at soft X-ray beamlines), a gap in the storage ring filling pattern, which is not foreseen in most low-emittance machines of the next generation and—in the specific case mentioned above—a special double slit geometry to switch between two separated beams.

In contrast, the method described in this study makes use of both a bunch-by-bunch or periodic turn-by-turn electron orbit variation and a separation in the time domain. Inherently, our new method offers helicity alternation rates in the MHz regime without any detrimental effect on the electron beam stability.

Results

General layouts. The basic idea of the scheme reported here uses the recently implemented option to store electron bunches on two different stable orbits in the so-called transverse resonance island buckets (TRIBs; see Methods)^{26–28} and to use an undulator to generate different helicities from the different orbits. In an ideal scenario, one would use a special cloverleaf-like magnetic structure (Fig. 1a) where electron bunches that pass on two canted orbits emit photon beams of opposite helicity. This scheme represents a particularly clean case, because the light from both orbits is emitted from the same source point in the center of the undulator and is focused automatically on the same spot of the sample. Intersecting beams in the center of the straight section is a matter of the electron optics that supports transversely separated beams.

However, a cloverleaf-like magnet design as in Fig. 1a does not exist yet and its design admittedly has to overcome considerably difficulties as strong field gradients are required to switch from the right to left circular field within a short lateral distance. Diffraction-limited light sources with round beams, small divergence, and small magnetic gaps will help in this aspect. Nevertheless, the maximum field is reduced compared with a conventional Advanced Planar Polarized Light Emitter-II (APPLE II) design and, furthermore, the intersection between the le- and right-handed array must be sufficiently long here to permit a clean separation of the electron beams and a proper shielding of the fields. Thinking about the feasibility with existing undulator designs, one might horizontally displace only one module of a twin APPLE undulator similar to that in Fig. 1b. Here, electron beams traverse the axes of separated helical magnet structures emitting light of opposite helicity if the shift parameters of the two APPLE II-type undulators¹⁰ are set to an opposite sign. Re-aligning one single undulator is quickly done, if the module is mounted on a remotely controllable motorized carriage. It is important to mention that the two sources are

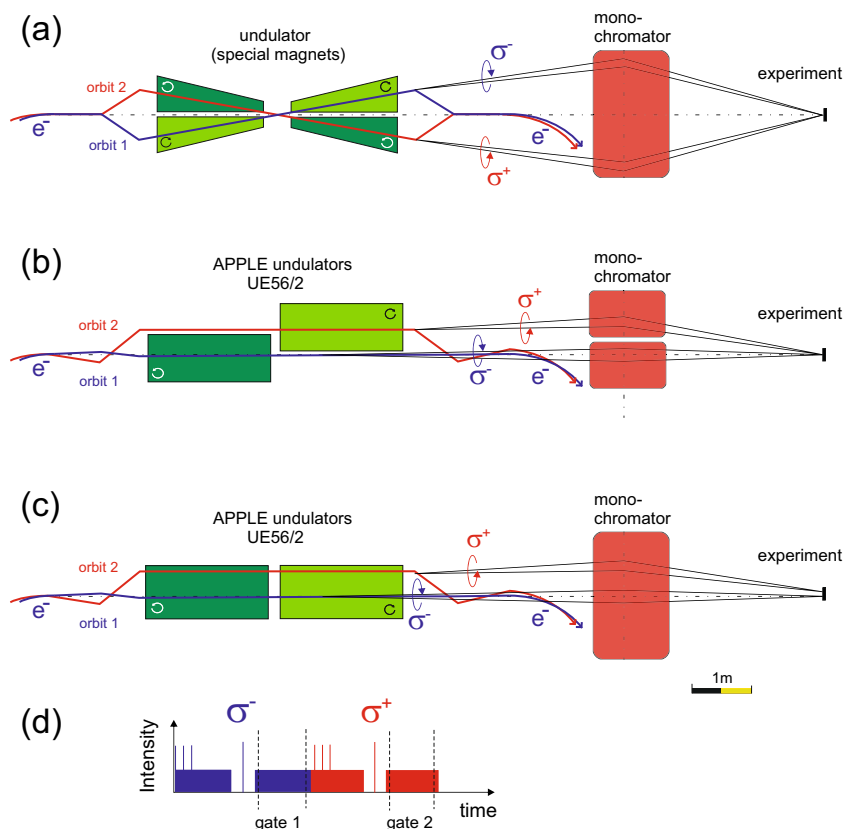


Fig. 1 Different schemes for fast helicity alternation from undulators. **a** Specific magnet configuration of an undulator and beamline supporting fast helicity alternation from electrons (e^-) traveling on different orbits (orbit 1 and orbit 2). The cloverleaf-like arrangement permits the production of right-handed (σ^-) and left-handed (σ^+) circular photons in the upstream (left) and downstream (right) undulator; thus, the highest flux is expected. One conventional monochromator focuses both beams on one spot at the sample. **b** Two Advanced Planar Polarized Light Emitter (APPLE) undulators UE56/2 are transversely displaced. The two resonant island orbits traverse the proper resonant undulator on axis. Two sets of optics are required to focus both beams on one spot. The flux is reduced by about a factor of two as compared with option **a**. **c** Arrangement of the proof-of-principle experiment reported here. The undulators are arranged in a line. Electrons on one island orbit traverse the resonant undulator at the center, the other one in the off-axis fringe field emitting opposite X-ray helicity from successive turns. **d** Signals from the corresponding filling patterns (first turn blue, second turn red) are selectable by variable temporal gate windows (gate 1 and gate 2), which are 800 ns apart.

longitudinally shifted and the beamline must accept and focus two strongly separated beams that would need two separated pre-mirror optics or require even two monochromators.

Pilot experiment at BESSY II. For our proof-of-principle experiment, we use a scheme that does not even require the displacement of an undulator. It is displayed in Fig. 1c (with fill patterns in Fig. 1d) and described in the following: if an on-axis electron beam passes two helical undulators with identical gap setting and opposite shift, the harmonics for both helicities appear at the same energy. Beams passing both devices with a lateral offset from the undulator axis will still produce identical harmonics in both undulators, but at a blue-shifted energy as simulated²⁹ in Fig. 2a and measured in Fig. 2b, because the electron beam propagates in the fringe fields (see Supplementary Note 1 and Supplementary Fig. 1). Figure 2 reveals that the blue shift is indeed considerable and amounts to ca. 20 eV at the Ni L_3 edge at only 3 mm horizontal offset (blue curve) at preserved degree of circular polarization of 60% (see also Supplementary Note 2 and Supplementary Fig. 2) By tuning the gap, we can compensate for this energy shift and move the harmonics back to the original energy of the on-axis beam. Our approach is based on a spectral separation of the two radiation cores using this energy shift.

Detuning only the gap of, e.g., the downstream device such that the off-axis beam emits the same photon energy as the on-axis beam in the upstream device (black line in Fig. 2a), the experiment sees in its narrow spectral window of $\Delta E = 200$ meV width at $E_{\text{ph}} = 852$ eV, determined by the monochromator, only light from the on-axis beam in the upstream device and from the off-axis beam in the downstream undulator. The harmonics from the other beams (off-axis in the upstream device and on-axis in the downstream one) are both shifted in energy out of the monochromator acceptance. Setting both APPLE II devices to opposite helicity with appropriate phasing¹¹, an on-axis beam in the upstream device will only emit one helicity and an off-axis beam in the downstream device the counter helicity. The experimental proof of this scheme is the subject of the present paper.

In all three schemes presented in Fig. 1, the electron bunches pass the two undulators on different trajectories, in the best case on a bunch-by-bunch basis resulting in 500 MHz helicity alternation rate or at least turn-by-turn, i.e., 1.25 MHz at BESSY II. In contrast to dynamic orbit bumps^{22,23} or phase shifters²⁴ by fast kickers, where the residual closed-orbit distortion sets a limit to the helicity alternation rate, we use a novel entirely static two-orbit operation mode based on TRIBs^{26–28}. In addition to the main orbit, which is defined by the center of all quadrupole magnets, a second stable island orbit is established at a horizontal

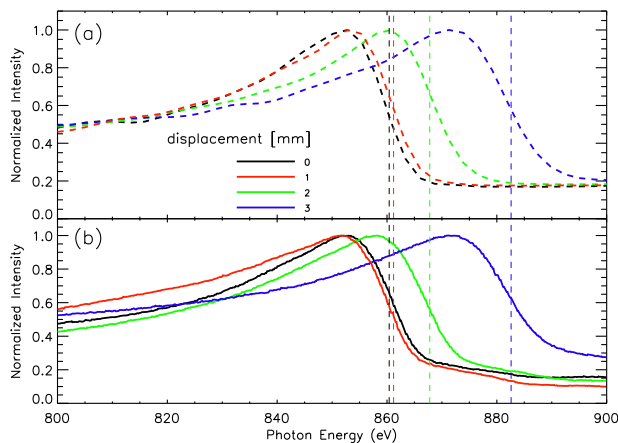


Fig. 2 Simulation and measurement of the third harmonic of the UE56 for different horizontal displacement of the electron beam. **a** Simulation of the undulator harmonic (normalized to its maximum) from the UE56/2 at shift 24 mm in vertical elliptical mode for different horizontal positions of the electron bunch in the BESSY II storage ring. The simulated degree of circular polarization defined as $P_c = |S_3/S_0|$, where S_3 and S_0 are the Stokes parameters, in the maxima is 60%. **b** Measurement of the harmonics for different horizontal displacements of the electron beam in the relevant BESSY II high beta straight section from 0 (on-axis) to 3 mm off-axis. The regular beam was found to be slightly misaligned to negative displacements with respect to the axis in **a** as indicated by the red and black dashed curve compared with the expectations **b**.

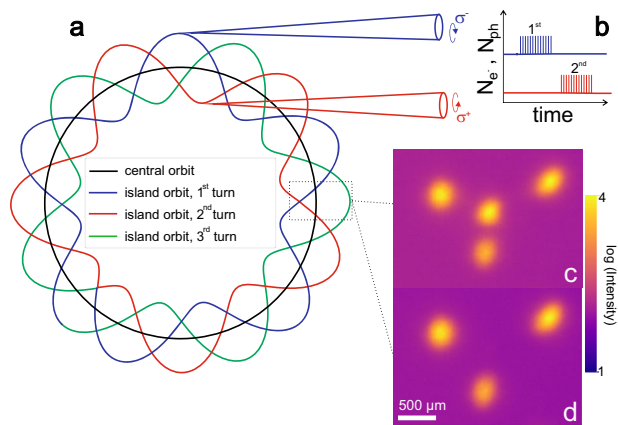


Fig. 3 Principle of bunch-by bunch or turn-by-turn helicity flip of elliptically polarized X-rays from an undulator in a storage ring using transverse island buckets from a third-order resonance. **a** Sketch of the electron orbit that closes after three turns passing the magnetic rows of a helical undulator at displaced position. **b** Thus, a number of photons N_{ph} of different helicity is emitted in time from a number N_{e^-} of electrons from the first (blue) and second turn (red). X-rays from the third turn (green in **c**) are blocked and not accepted by the beamline. **c** Hard X-ray pinhole camera image of the four source points in a dipole observed when the core beam and the islands are populated by the same number of electrons and **d** when only the island orbit is populated.

third-order resonance winding around the main orbit in the horizontal plane and closing after three revolutions, as depicted in Fig. 3a and their temporal x-ray emission in Fig. 3b. This way, three additional island buckets, i.e., potential wells, are generated where electrons can be stored.

Both orbits have different tunes and can simultaneously be populated with electron bunches as in Fig. 3c. Moreover, by a resonant tune excitation, electron bunches can be pushed from

one orbit to the other one without losing charge. The hard X-ray source image from a dipole in Fig. 3d shows the situation when all electron bunches are stored on the island orbit. It is noteworthy that the vertical distance of the three source points observed in a dipole practically vanishes in the straight section (by 2% coupling, see Supplementary Note 3 and Supplementary Figs. 3 and 4).

There are two modes to populate the island orbit with electron bunches: (i) individual bunches from the main orbit (black) are divided in equal parts onto the three island buckets (1-blue, 2-red, 3-green), resulting in three almost equally charged bunches passing a beamline within the same time window. A beamline that only accepts one single island spot will see each turn a signal reduced by 1/3, but from different bunches (i.e., 1,2,3,1,2,3 etc.). (ii) Alternatively, the entire charge of the main orbit bunch (black) is pushed into only one island bucket (e.g., the blue one from Fig. 3). Then, a beamline accepting only one island spot will see a full signal only every third turn. Such Single Island Population (SIP) has already been used at the Metrology Light Source to increase the revolution time for time-of-flight electron spectroscopy experiments³⁰.

Combining the twin undulator setup (Fig. 1c) with the TRIBs and electrons stored in the islands, there are two different scenarios possible as depicted in Fig. 3: (i) selected bunches, e.g., successive ones, are populated alternately in the core orbit and in the islands at about the same bunch charge. If one accepts one of the permanently populated islands and the core beam in the beamline, then both would emit alternately opposite helicity with 500 MHz flip rate (2 ns). (ii) SIP mentioned above with all bunches (the complete fill pattern) in the ring leads to a closed orbit of this macro-pulse only after three turns as in Fig. 3 and, as indicated by blue and red radiation cones, a turn-by-turn flip of the helicity after 800 ns between the first and second turn (see fill patterns in Fig. 1d) but with 800 ns break if the green third turn is not accepted like in the present case. As a detection with <2 ns time resolution was not available in our current setup to address scenario (i), we used a nearly complete filling of the BESSY II ring (50 mA, 350 of 400 possible bunches) and demonstrate the proof-of-principle of method (ii) as follows.

Turn-by-turn detection of the helicity change. To detect the X-ray helicity, we use the XMCD effect in a Permalloy ($\text{Ni}_{80}\text{Fe}_{20}$) sample that we magnetized along the beam direction using an electromagnet. As described in the Methods section, the X-ray signal transmitted through the sample is detected with a fast avalanche photo diode (APD); the signal from the first and second revolution is temporally sorted using a digital oscilloscope. As there is no beamline capable of focusing on-axis and off-axis beam simultaneously on the same spot, we use the first mirror M_1 (Supplementary Note 4 with optical layout in Supplementary Fig. 5) of the beamline to horizontally steer either one or the other beam on the sample. Figure 4a, b show the signals (and Fig. 4c, d the corresponding magnetic asymmetry) transmitted through the sample as a function of the angular position of the M_1 -mirror in the undulator arrangement including gap detuning (by 1.1 mm) and opposite shifts (phases) of ± 24 mm described above. As the mirror M_1 (at 17 m) images the source on a scale of ca. 1 : 1, the horizontal offset of the electron beam from the first and second revolution is directly measured here as $\Delta x = 3.7$ mm (distance of the 2 peaks in Fig. 4). By alternating the out-of-plane magnetization (+, -) of the sample with the photon energy tuned to the Ni L_3 resonance, it is possible to estimate the X-ray helicity emitted by the two source points. As shown in Fig. 4c, the magnetic contrast between the two subsequent turns (i.e., the two source points) is obviously reversed. The sign of the magnetic contrast is reversed in the right graph of Fig. 4d upon flipping the

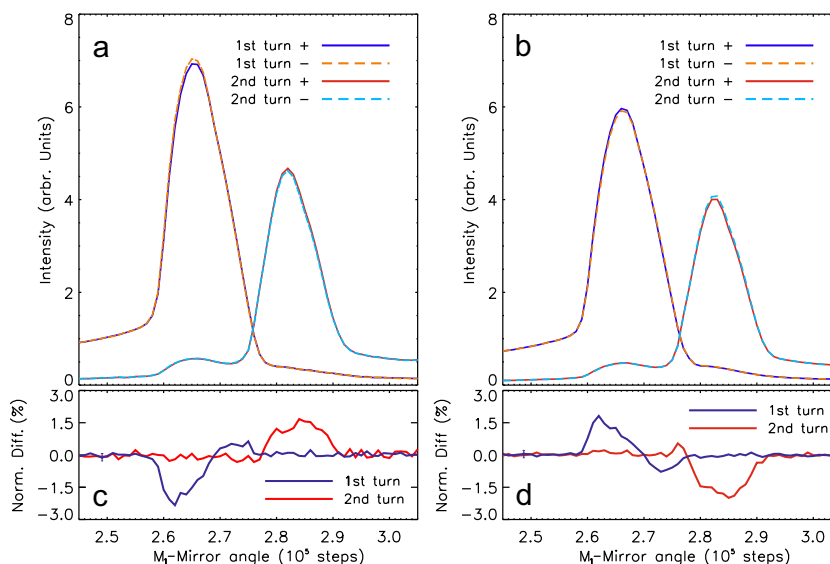


Fig. 4 Mapping of the intensity behind the sample at $E_{ph} = 852$ eV in the image plane by angular scans of the mirror M1 of the beamline.

a Downstream shift +24 mm and upstream shift -24 mm. **b** Sign of both shift parameters flipped. The intensity of both beams, owing to the available beamline layout, is different, because the downstream device (left peak) produces higher flux than the upstream one (right peak), as its center is closer to the observer (depth of field effect). **c, d** Normalized difference signals from the first and second turn when alternating the magnetization of the sample (+, -). The relative magnetic contrast (Norm. Diff.) changes its sign, indicating the turn-by-turn flip of the helicity. Compensating effects in the overlap region between the two peaks (light cones) show reversed helicity.

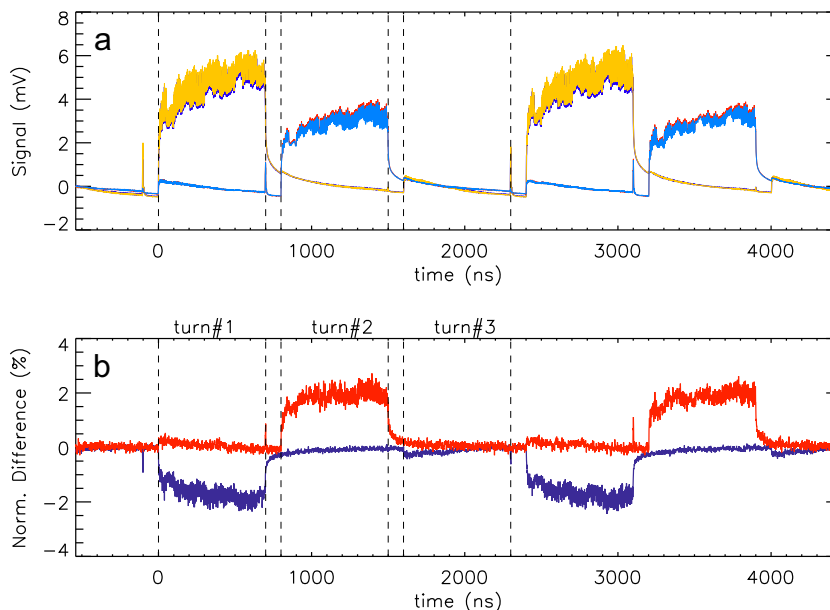


Fig. 5 Temporal waveforms of intensity and asymmetry from the first three turns of all bunches in the ring. **a** Oscilloscope traces from the avalanche photo diode (APD) detector measured on island 1 (orange, blue) and island 2 for an out-of-plane magnetic field strength of $B = -0.5$ to 0.5 T (pale blue and red), respectively. **b** The small intensity differences in **a** become evident in the normalized difference signal (magnetic contrast), which indicates the helicity flip between first (blue) and first turn (red). There is no dichroic signal at the third turn since island 3 is not accepted by the beamline. It is noteworthy that a single bunch filled 100 ns before the macro bunch likewise shows a turn-by-turn helicity flip of its X-ray emission, useful for pump-probe applications^{4,5}.

shift parameters of downstream and upstream device according to the layout Fig. 1c.

The same information in time domain is shown in Fig. 5. Here, the traces show the raw signals emitted from the SIP with a special filling of a long macro-pulse and with a single bunch arriving 100 ns before the macro-pulse (Supplementary Note 5 and Supplementary Figs. 6 and 7). The corresponding maximum magnetic contrast $A = (I^+ - I^-)/(I^+ + I^-)$ shows

that bunches from the first and second revolution emit here the opposite helicity. Using a benchmark XMCD measurement of the same sample from a bending magnet beamline PM3 that yielded $A = 7.4\%$ corresponding to a circular polarization $|S_3/S_0| = 75\%$ (see Supplementary Note 6 and Supplementary Fig. 8), we find here that the bunch train in Fig. 5 with $A = (2.5 \pm 0.5)\%$ emits values of $|S_3/S_0| = (25 \pm 5)\%$ in the TRIBs setting.

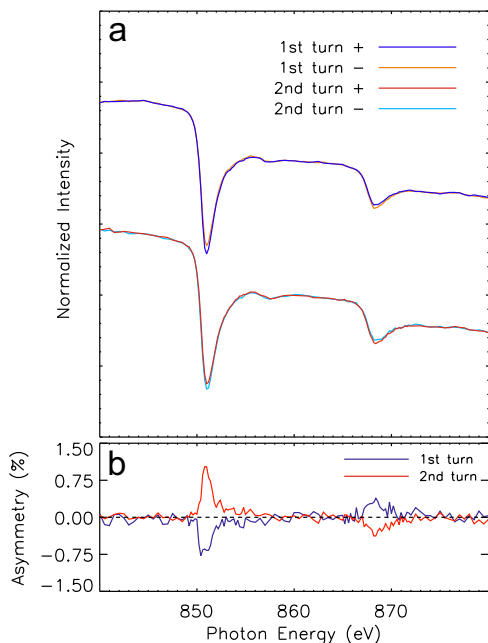


Fig. 6 **A typical X-ray circular dichroism (XMCD) measurement using the gated detector signal from first and second turn for both magnetization directions of the sample.** **a** XMCD spectra normalized to the 800 eV value and shifted for clarity across the L_3 and L_2 , $2p \rightarrow 3d$ resonances of Nickel in the Permalloy sample and the corresponding magnetic contrast (asymmetry) **b** from the first (blue) and second turn (red). Here, the signals (mean values) from the corresponding gate windows set to the first and second turn are acquired for the two different magnetization directions (+) and (−), parallel and antiparallel orientation of the pointing vector of X-rays and out-of-plane sample magnetization vector, respectively.

According to the simulations in Fig. 2, Fig. 5 we expect from the individual undulators $|S_3/S_0| = 60\%$ but measure less than half of this value. The reason for this is the small horizontal separation, which causes transverse and spectral overlap effects of the radiation cones, as proven by simulations using the code named WAVE²⁹ with particle tracking along the magnetic field gradient (see Methods). In our setting, we could not further increase the horizontal distance of the two source points because of the limited horizontal acceptance of the existing beamline. There are, however, two straightforward technical solutions to improve $|S_3/S_0|$: (i) increase of the horizontal acceptance of the beamline or (ii) a double slit aperture in the front end to accept only the individual undulator cones, to clip red shifted fringes. In a dedicated setup at a diffraction-limited light source, the overlap reductions will be naturally alleviated by a much lower emittance and a point-like source.

To demonstrate a usual XMCD measurement at the selected settings, the mean values of the signals from the first and second gate windows of Fig. 5 were now displayed in Fig. 6 during an energy scan (combined undulator-monochromator ride with magnetic field alternation). The XMCD difference-over-sum signal clearly shows that the helicity is reversed between the two turns. It is noteworthy that at an optimized beamline the two spectra for one magnetization would be recorded quasi-simultaneously with only an 800 ns time delay of the acquisition gate windows and both would have the same incident photon flux. The absolute averaged $|S_3/S_0|$ at the Ni L_3 resonance energy is $<25\%$ here, because the mean value of the macro-pulse from Fig. 5 shows some background effects of the APD (slow fall time) and, likewise, owing to a finite population purity (see Methods/TRIBs). Similar to the limited acceptance mentioned above, this technical issue can also be solved with a dedicated beamline and at faster detection.

Discussion

To conclude, we provided the first demonstration of a turn-by-turn flip of the X-ray helicity from an electron storage ring, which is the highest alternation frequency from an undulator in a storage ring ever reported. The experiment further demonstrated that a stable operation of a low-emittance light source under TRIBs settings combined with state-of-the-art helical undulator technology at diffraction-limited light sources, currently coming to life worldwide, might open new insights into the physics of magnetic materials at ultimate signal-to-noise and time resolution.

Methods

Beamline and circular dichroism. To probe the helicity of X-rays from the undulator, the UE56-2 PGM2 beamline³¹ was used with the third harmonic from the twin APPLE II undulator UE56-2 at a shift parameter of ± 24 mm in the range of 700–900 eV at a resolution of $\Delta E = 200$ meV (1200 l/mm grating) addressing XMCD in transmission at the Nickel L_3 and L_2 absorption edges (Ni, $2p_{3/2} \rightarrow 3d$, $2p_{1/2} \rightarrow 3d$), respectively. For spectral separation, the downstream undulator was set to a gap of 26.024 mm and the upstream on to 27.124 mm tuning the third harmonic of both devices to the Ni L_3 transition $2p_{3/2} \rightarrow 3d$, i.e. $E_{ph} = 852$ eV photon energy. For energy scans across L_3 and L_2 , both gap motors were driven in parallel with the spectral window of $\Delta E = 200$ meV of the monochromator. This beamline is a plane grating monochromator³¹ (see Supplementary Fig. 5) specially designed for large horizontal angular acceptance of ≈ 1 mrad as determined by the first mirror and ≈ 4 mm horizontal acceptance (given by the refocusing mirror) with respect to the source displacement. It is important to note that the first toroidal mirror M1 produces horizontally a $\approx 1:1$ image of the source point(s) on the detector.

A dedicated XMCD endstation³ allowing for magnetizing the sample with up to $B = \pm 0.5$ T is used. The detection employs a silicon APD (SAR 3000 from Laser Components) together with a 4 GHz oscilloscope (LeCroy) and a trigger hardware fed by the 500 MHz RF master clock frequency, which divides the bunch clock of 1.25 MHz (revolution frequency) by a further factor of 3 to detect average standing waveforms of the APD signal from three subsequent revolutions. As specimen, a magnetron-sputtered thin film of 15 nm-thick $\text{Ni}_{80}\text{Fe}_{20}$ (Permalloy) on a $0.5 \mu\text{m}$ freestanding Aluminum foil of 4 mm diameter was used in normal incidence at out-of-plane magnetization \vec{M} by the external axial magnetic field along the pointing vector \vec{S} of the X-rays. The sample was benchmarked previously at the PM3 beamline at BESSY II, a plane grating monochromator on a dipole magnet optimized for XMCD experiments³². To detect the helicity and estimate the polarization degree, we use the fact that for a thin film, the magnetic contrast $A = (I^+ - I^-)/(I^+ + I^-)$ at the resonances is proportional to $|S_3/S_0|$, where I^+ and I^- are the transmitted intensities for \vec{M} parallel or antiparallel to \vec{S} , respectively. A maximum XMCD signal from that sample of $A = 7.4\%$ at the Ni L_3 edge was found here corresponding to $|S_3/S_0| = 75\%$ degree of circular polarization (see Supplementary Note 6).

Accelerator settings and transverse island buckets. The main orbit in storage rings is defined by the center of all quadrupole magnets, which focus off-center particles in the transverse planes leading to betatron oscillations in the x and y plane at fixed frequencies. The number of these oscillations is called tune and typically chosen not to be in resonance with the revolution of the storage ring; since then, magnetic errors and/or misalignments would sum up turn-by-turn and drive the beam to large amplitudes until it is lost at an aperture. At BESSY II, the tunes are chosen to be $(Q_x, Q_y) = (17.848, 6.724)$ for the standard user optics. For the TRIBs optics^{26,27}, the storage ring is operated in the present case close to the third-order integer resonance $Q_{x\text{Resonance}} = 17.666$ and, by a special setting of the nonlinear sextupole magnets, three additional so-called resonant island buckets appear in the horizontal phase space in addition to the main bucket (main orbit), representing a second stable “island” orbit closing after three revolutions as depicted in Fig. 3 (in more detail in Supplementary Fig. 4). Both beams have different tunes and for this experiment $Q_{x\text{Core}} = 17.649$, $Q_{x\text{Island}} = 17.684$, and separated by³³ $Q_{x\text{Resonance}} = 17^2/3$. The tune deviation defines the separation of both orbits, which results in displacements of -4.4 mm, 4.5 mm, and 1.0 mm of the three folded island orbit (in the relevant straight section) as shown in the Supplementary Fig. 3. There is a minimum tune separation causing both beams to merge, because then the orbit/bucket separation becomes smaller than the equilibrium beam emittance. Likewise, there is a maximum tune separation, where electrons from the island orbit get lost far off-axis. Displacements far beyond 10 mm are possible at BESSY II. The equilibrium beam emittance for the main orbit in the TRIBs setting is nearly the same as for the standard user setting $\epsilon_x = 7$ nmrad, whereas the emittance of the TRIBs orbit is slightly increased at a small separation to $\epsilon_x = 8$ nmrad and can further rise by up to $\epsilon_x = 12$ nmrad at large separation³³.

As both orbits have different tunes, a bunch-by-bunch resolved resonant tune excitation, in our case generated with the Bunch-by-Bunch Feedback System^{34,35}, can be used to populate and depopulate the orbits with electron bunches. By exciting each turn resonantly at the tune of a bunch of the main orbit, the particles

are driven to higher transverse oscillation amplitudes leaving the main bucket getting equally captured in the three island buckets. Exciting the bunches on the island orbit, only two of three turns will push them back to the main orbit leading to a SIP^{26,33}. For the proof-of-principle experiment described here, the ring was filled with 350 of 400 buckets at an injected current of $I = 50$ mA in decay mode with a lifetime of ~ 15 h. A good SIP of about 85% purity was reached with 10% and 5% residual charge captured in the other two island buckets (see Fig. 5). Tuning the separation of the TRIBs optics, the displacement and angle of the electron beam in the straight section can be changed such that undulator light from the selected islands points into the beamline. In the present case, a slight reduction to 3.7 mm distance as measured from Fig. 4 between the first and second turn with respect to the standard setting of 5.4 mm (see Supplementary Fig. 3), -4.4 mm and $+1.0$ mm) was necessary to accept X-rays from two turns assisted by a horizontal local orbit bump of $x = 1$ mm and $x' = -0.14$ mrad.

Numerical simulation of undulator radiation from TRIBs. The numerical calculation of the spectral flux S_0 and polarization degree expressed as Stokes parameter ratio $|S_3/S_0|$ have been carried out with the code WAVE²⁸. The magnetic field of the undulators was calculated for a model of permanent magnet blocks, as it exists in reality at the two UE56 undulators (30 periods) including fringe fields. The field of each block is evaluated via the current sheet method and the remanence value of the magnets was slightly adjusted here to be consistent with the measured photon energy of the third on-axis harmonic of the UE56 at the Ni L_3 absorption edge of $E_{ph} = 852$ eV. The beam emittance of $\epsilon_x = 8$ nmrad at an energy spread of $\delta\gamma/\gamma = 7 \times 10^{-4}$ at $\gamma = 1.72$ GeV electron energy of the TRIBs electron optics in BESSY II have been taken into account by tracking 10^5 electrons generated randomly from the appropriate phase-space distribution. To speed up calculations for each electron, a single transverse photon observation point has been randomized within the experimentally used aperture of horizontal ± 15 mm and vertical of ± 1 mm at 11 m from the source point (aperture plane). The vertical elliptical mode at shift 24 mm, the large angular acceptance (of red shifted radiation) together with a larger horizontal source size in the high β -sections, then lead to a theoretical degree of circular polarization of $|S_3/S_0| \approx 60\%$ at the maximum of the third harmonic at $E_{ph} = 852$ eV (see Supplementary Fig. 2).

Data availability

The data that support the findings of this study are available from the corresponding author upon reasonable request.

Received: 20 February 2020; Accepted: 10 March 2020;

Published online: 01 April 2020

References

- Schütz, G. et al. Absorption of circularly polarized X-rays in iron. *Phys. Rev. Lett.* **58**, 737–740 (1987).
- Chen, C. T. et al. Soft-X-ray magnetic circular dichroism at the L_{2,3} edges of nickel. *Phys. Rev. B* **42**, 7262–7265 (1990).
- van der Laan, G. & Figuerosa, A. I. X-ray magnetic circular dichroism. *Coord. Chem. Rev.* **277–278**, 95–129 (2014).
- Stamm, C. et al. Femtosecond modification of electron localization and transfer of angular momentum in nickel. *Nat. Mater.* **6**, 740–743 (2007).
- Radu, I. et al. Transient ferromagnetic-like state mediating ultrafast reversal of antiferromagnetically coupled spins. *Nature* **472**, 205–208 (2011).
- Mannini, M. et al. Quantum tunnelling of the magnetization in a monolayer of oriented single-molecule magnets. *Nature* **468**, 417–421 (2010).
- Schierle, E. et al. Cycloidal order of 4f moments as a probe of chiral domains in DyMnO₃. *Phys. Rev. Lett.* **105**, 167207 (2010).
- Martins, M. & Wirth, W. Magnetic properties of supported metal atoms and clusters. *J. Phys. Condens. Matter* **28**, 503002 (2016).
- Kowalska, J. K. et al. X-ray magnetic circular dichroism spectroscopy applied to nitrogenase and related models: experimental evidence for a spin-coupled molybdenum(III) center. *Angew. Chem. Int. Ed.* **58**, 9373–9377 (2019).
- Chen, C. T. et al. Experimental confirmation of the X-ray magnetic circular dichroism sum rules for iron and cobalt. *Phys. Rev. Lett.* **75**, 152–155 (1995).
- Bährdt, J. in *Synchrotron Light Sources and Free-Electron Lasers* (eds. Jaeschke, E. et al.) 1–84 (Springer Nature, Switzerland AG, 2019).
- Woo, S. et al. Observation of room temperature magnetic skyrmions and their current-driven dynamics in ultrathin Co films. *Nat. Mater.* **15**, 501–506 (2016).
- Hettel, R. O. Beam stability at light sources. *Rev. Sci. Instrum.* **73**, 1396–1401 (2002).
- Suzuki, M., Kawamura, N. & Ishikawa, T. Application of optical scanner to switching of X-ray photon helicities at kHz range. *Rev. Sci. Instrum.* **74**, 19–22 (2003).
- Gluskin, E. APS insertion devices: recent developments and results. *J. Synchr. Rad.* **5**, 189–195 (1998).

- Ivanushenkov, Y. et al. Conceptual design of a novel scape undulator. In *Proc. Intern. Part. Accelerator Conf. IPAC 17* 1596–1598 <https://doi.org/10.18429/JACoW-IPAC2017-TUPAB117> (Copenhagen, Denmark, 2017).
- Onuki, H. et al. Polarizing undulator with crossed and retarded magnetic fields. *Rev. Sci. Instrum.* **60**, 1838–1841 (1989).
- Singh, O. et al. Orbit compensation for the time varying elliptically polarized wiggler. *Rev. Sci. Instrum.* **67**, 3346 1–3346 6 (1996).
- Elleaume, P. HELIOS: a new type of linear/helical undulator. *J. Synchr. Rad.* **1**, 19–26 (1994).
- Bährdt, J. et al. Elliptically polarizing insertion devices at BESSY II. *Nucl. Instrum. Methods Phys. Res. A* **467–468**, 21–29 (2001).
- Schmidt, T. et al. Insertion devices at the Swiss light source (phase I). *Nucl. Instrum. Methods Phys. Res. A* **467–468**, 126–129 (2001).
- Hara, T. et al. Helicity switching of circularly polarized undulator radiation by local orbit bumps. *Nucl. Instrum. Methods Phys. Res. A* **498**, 496–502 (2003).
- Shirasawa, K. et al. Fast helicity switching of circularly polarized light using twin helicalundulators. In *Proc. Conf. Synchr. Rad. Instr. SRI 2003, San Francisco, USA, AIP Conference Proceedings 705*, 191–194 <https://doi.org/10.1063/1.1757766> (2004).
- Kinjo, R. & Tanaka, T. Spectrum splitting for fast polarization switching of undulators. *J. Synchr. Rad.* **23**, 751–757 (2016).
- Förster, D. et al. Phase-locked MHz pulse selector for X-ray sources. *Opt. Lett.* **40**, 2265–2268 (2015).
- Cappi, R. & Giovannozzi, M. Novel method for multiturn extraction: trapping charged particles in islands of phase space. *Phys. Rev. Lett.* **88**, 104801 (2002).
- Ries, et al. Transverse resonance island buckets at the MLS and BESSY II. In *Proc. Intern. Part. Accelerator Conf. IPAC 15* 138–140 <https://doi.org/10.18429/JACoW-IPAC2015-MOPWA021> (Richmond, USA, 2015).
- Goslowski P. et al. Two orbit operation at Bessy II - during a user test week. In *Proc. Int. Particle Acc. Conf. IPAC 2019* 3419–3422 <https://doi.org/10.18429/JACoW-IPAC2019-THYYPLM2> (Melbourne, Australia, 2019).
- Scheer, M., WAVE - A computer code for the tracking of electrons through magnetic fields and the calculation of spontaneous synchrotron radiation. In *Proc. Int. Computational Acc. Phys. Conf. ICAP12* 86–88 <http://accelconf.web.cern.ch/AccelConf/ICAP2012/papers/tuacc2.pdf> (Rostock-Warnemünde, 2012).
- Arion, T. et al. Transverse resonance island buckets for synchrotron-radiation based electron time-of-flight spectroscopy. *Rev. Sci. Instrum.* **89**, 103114 (2018).
- Sahwney, K. J. et al. A novel undulator-based PGM beamline for circularly polarised synchrotron radiation at BESSY II. *Nucl. Instrum. Methods Phys. Res. A* **390**, 395–402 (1997).
- Kachel, T., Eggenstein, F. & Follath, A. Soft X-ray plane-grating monochromator optimized for elliptical dipole radiation from modern sources. *J. Synchr. Rad.* **22**, 1301–1305 (2015).
- Kramer, F. et al. Characterization of the second stable orbit generated by transverse resonance island buckets (TRIBs). In *Proc. Int. Particle Acc. Conf. IPAC 2018* 1656–1659 <https://doi.org/10.18429/JACoW-IPAC2018-TUPML052> (Vancouver, Canada, 2018).
- Teytelman, D. et al. Architecture and technology of 500 M sample/s feedback systems for control of coupled-bunch instabilities. In *Proc. Int. Conf. On Accelerator and Large Experimental Physics Control Systems ICALEPCS 99* 252–254 (Trieste, Italy, 1999).
- Schälicke, A. et al. Bunch-by-bunch feedback and diagnostics at BESSY II. In *Proc. Int. Beam Instrumentation Conf. IBIC 13* 399–402 (Oxford, UK, 2013).

Acknowledgements

Financial support by: Bundesministerium für Forschung und Technologie of the German government. We are indebted to I. Radu (Max Born Institute) and F. Radu (HZB) for providing us with Permalloy and Ni thin-film specimen as useful probes for circular polarization. We thank Dirk Ponwitz for technical support and J. Viehhaus, G. Reichardt, T. Zeschke, F. Eggenstein, and F. Senf and others for useful information about the UE56–2 PGM2 beamline. We particularly thank A. Vollmer and F. Staier, who made the dedicated beamtime in TRIBs optics possible for us, and G. Wüstefeld who proposed to use TRIBs at BESSY II.

Author contributions

K.H. and J.B. conceived the research. P.G., F.A., M.R., and A.S. set up the accelerator and are developers of the TRIBs electron optics. K.H., C.S.-L., P.G., and J.B. performed the experiments with contributions from N.P. and W.F. M.S. simulated the undulator spectra. C.S.-L. and K.H. measured polarization benchmarks with contributions from T.K. J.B. and W.F. prepared undulator settings and operation. K.H., J.B., P.G., and C.S.-L. wrote the manuscript with contributions from all authors.

Competing interests

The authors declare no competing interests.

Additional information

Supplementary information is available for this paper at <https://doi.org/10.1038/s42005-020-0331-5>.

Correspondence and requests for materials should be addressed to K.H. or J.B.

Reprints and permission information is available at <http://www.nature.com/reprints>

Publisher's note Springer Nature remains neutral with regard to jurisdictional claims in published maps and institutional affiliations.



Open Access This article is licensed under a Creative Commons Attribution 4.0 International License, which permits use, sharing, adaptation, distribution and reproduction in any medium or format, as long as you give appropriate credit to the original author(s) and the source, provide a link to the Creative Commons license, and indicate if changes were made. The images or other third party material in this article are included in the article's Creative Commons license, unless indicated otherwise in a credit line to the material. If material is not included in the article's Creative Commons license and your intended use is not permitted by statutory regulation or exceeds the permitted use, you will need to obtain permission directly from the copyright holder. To view a copy of this license, visit <http://creativecommons.org/licenses/by/4.0/>.

© The Author(s) 2020